Weak and strong coupling properties of surface excitons

Arpan Dutta[1, 2, *] and J. Jussi Toppari[1, †]

[1] *Nanoscience Center and Department of Physics, University of Jyväskylä, 40014 Finland*
[2] *Department of Mechanical and Materials Engineering, University of Turku, 20014 Finland*

With high enough doping concentrations, organic dye doped polymer materials exhibit negative real part of the permittivity within an energy range just above their material absorption, incurring surface exciton modes at these energies. Here, we report how such modes can be used to realize strong light-matter coupling with photoactive molecules. Our simulations reveal that surface excitons can facilitate strong coupling by sustaining the energy-splitting-induced transparency, however, the polaritons may not be visible in the absorption since they can easily be located outside of the narrow negative permittivity regime. Moreover, we show that the surface exciton modes cannot couple strongly with the surface plasmons. Our findings shed light on the weak and strong coupling properties of surface excitons.

Introduction. Interaction between light and matter, mediated via optical nanostructures, is of great interest in modern resonant nanophotonics [1]. Plasmonic (*i.e.*, metallic) nanostructures are widely utilized in such studies due to their unique capability of confining and enhancing light [2–7]. However, absorption losses are usually high in metals and often limit the optical performance of plasmonic systems. To overcome this problem, a quest has emerged for alternative materials possessing *metal-like* behaviour with low losses, especially in the visible range [8, 9]. Polymer materials doped with organic dyes having Frenkel excitons are an important class of such materials since if the doping concentration is high enough, these excitonic materials can sustain surface exciton (SE) modes at room temperature that are analogous to the surface plasmon (SP) modes in metals [8–19]. Like SP modes, SE modes can be exploited in refractive-index sensing [13, 19] and in near-field enhanced spectroscopy [17, 19]. Moreover, SE modes possess lower material losses compared to SP modes [8] and unlike SPs, their optical performance can be tuned by varying the doping concentration [19].

The origin of SE modes in excitonic materials can be understood by looking into the real part of their dielectric function ($Re\{\epsilon(\omega)\}$). In metals, SP modes can exist only in the spectral region where $Re\{\epsilon(\omega)\} < 0$ [8, 9]. For noble metals such as gold (Au) [20], this negative $Re\{\epsilon(\omega)\}$ region is very broad covering all the energies below ~ 5.96 eV, as one can see in Fig. 1(a). In dye doped polymers such as polyvinyl alcohol (PVA) doped with TDBC J-aggregates, when the doping concentration is high enough, $Re\{\epsilon(\omega)\}$ becomes negative within a narrow spectral window at energies just above the material absorption of TDBC (2.08 eV) as shown in Fig. 1(b) [9, 12–17, 19]. This narrow spectral window ($\sim 2.1 - 2.3$ eV in Fig. 1(b)) where $Re\{\epsilon(\omega)\} < 0$ can be considered as a surface mode region (SMR) and the SE modes can only exist within it [19]. Similarly, we can define SMR

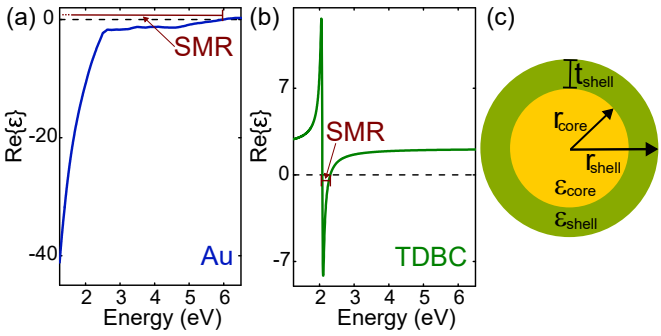

FIG. 1. Real part of the dielectric function ($Re\{\epsilon(\omega)\}$) of (a) Au [20] and (b) PVA doped with high concentration of TDBC J-aggregates, as a function of energy. The excitonic TDBC material is modeled using Eq. (1) explained in the text, with the same parameters as used in Fig. 2(b). The surface mode region (SMR), i.e., the spectral range where $Re\{\epsilon(\omega)\} < 0$ and thus the surface modes, SPs or SEs, are supported, is marked for the both materials. (c) Core-shell nanoparticle geometry where core radius $r_{core} = 50$ nm, shell thickness $t_{shell} = 25$ nm, and shell outer radius $r_{shell} = 75$ nm. The complex-dispersive dielectric functions of the core and shell materials are $\epsilon_{core}(\omega)$ and $\epsilon_{shell}(\omega)$, respectively.

for Au, i.e., spectral region supporting SPs, as shown in Fig. 1(a). In excitonic materials, which support SE modes, SMR directly depends on the transition dipole moment, i.e., oscillator strength (f), and the absorption linewidth (γ) of the dopant (e.g., TDBC), and can be modified by varying the doping concentration [19, 21]. Consequently, only organic molecules that have strong transition dipole moment along with narrow absorption linewidth can sustain such SE modes and have SMR with non-zero bandwidth [8, 19].

Existing theoretical [13–17, 19] and experimental [8, 9, 12, 18, 21] studies on organic nanostructures mainly focus on realizing different SE modes, and using them as sensors and resonant substrates when the light-matter coupling is weak. Use of SE modes as the so-called *cavity mode* in strong light-matter coupling [22] is not well investigated and not even considered as per author's knowledge. Considering this research gap, our research ques-

* arpan.dutta@utu.fi
† j.jussi.toppari@jyu.fi

tion in this letter is *can we utilize SE modes to facilitate strong light-matter coupling similarly as with SP modes?* To explore that we perform numerical simulations where SE modes are used as the platform for strong coupling. We also compare the scenario of SE modes to a similar case of SP modes. We further examine the coupling between SE and SP modes to explore light coupling properties of SEs.

To facilitate strong light-matter coupling, we consider a core-shell nanoparticle (NP) geometry as shown in Fig. 1(c). The core radius (r_{core}) is considered to be 50 nm while the shell thickness (t_{shell}) is taken as 25 nm leading to a shell outer radius (r_{shell}) of 75 nm. The complex-dispersive dielectric functions of the core and shell materials are $\epsilon_{core}(\omega)$ and $\epsilon_{shell}(\omega)$, respectively.

Coupling between organic molecules and SP. At first, we consider a gold (Au) core with a generic dye shell to study strong light-matter coupling between organic molecules and the SP mode as a reference case. The dielectric function of the Au core ($\epsilon_{core}(\omega)$) is obtained from the literature [20], while the permittivity of the dye shell ($\epsilon_{shell}(\omega)$) is modelled using the Lorentz oscillator model (LOM) [9, 19, 21]. For details on the Lorentz permittivity, see Supplemental Material [23].

In LOM, the dielectric function is expressed as

$$\epsilon(E) = \epsilon_\infty + \frac{fE_0^2}{(E_0^2 - E^2 - i\gamma E)}, \tag{1}$$

where $E = \hbar\omega$ is the energy, ϵ_∞ is the dielectric constant of the host polymer, f is the oscillator strength of the molecular absorption having E_0 as its spectral peak position and γ as its spectral linewidth. For the generic dye shell, we consider $\epsilon_\infty = 1.45^2$ and $\gamma = 0.1$ eV since these numbers correspond well to the realistic dyes [24]. The spectral peak E_0 is set to 2.28 eV to have a spectral match with the absorption maximum of the SP mode of the gold core (E_c). The change in molecular concentration of the shell is modelled by varying f (f_{dye}) as 0.01, 0.03, 0.05, 0.10, 0.15, and 0.20.

The optical properties of the core-shell NP are calculated using Mie theory [25] implemented in MATLAB [26] since the NP size is beyond the quasi-static limit [27]. For details on the Mie calculations, see Supplemental Material [23]. We examine the absorption (absorption efficiency, *i.e.*, absorption cross-sections normalized by geometrical cross-section) of the core-shell system since signature of strong coupling is more clearly manifested in that than in the scattering or extinction [28, 29]. The black and red curves in Fig. 2(a) show the absorption of the plain dye shell and sole Au core, respectively, with a spectral tuning of the dye at $E_c = 2.28$ eV. For the coupled system, an increase in f_{dye} incurs a rise in the energy splitting, *i.e.*, an increase in the energy separation between the upper (UP) and lower (LP) polariton branches as shown in Fig. 2(a). Such finding is consistent with the earlier reports on plasmon-molecule strong coupling in core-shell systems [24, 28–31]. The appearance of the polaritons and Rabi split in the absorption spectrum is a clear signature of the strong coupling [22], which we consider as its main criterion for now on.

In Fig. 2(a), we also see that for high values of f_{dye} (0.10, 0.15, and 0.20), an absorption peak reappears around E_c. In the absorption of the strongly coupled core-shell system, one should expect to see lowering of the absorption, at E_c with two polariton modes (UP and LP) emerging at the red and blue side of it [24]. However, emergence of this middle peak at the resonance energy E_c for $f_{dye} \geq 0.10$ is consistent with the earlier reports [28, 32, 33]. It has been shown by classical approach [28] as well as using quantum mechanics [32] that this middle peak emerges due to the absorption of uncoupled, i.e., non-hybridized, molecules in the case of exact resonance between the SP mode and molecular absorption with very high oscillator strength, and especially in the case of thick dye layers. Recently, it has been shown by a heuristic quantum model [33] that this middle peak at resonance (E_c) exists in the absorption of strongly-coupled core-shell system when simulated via Mie theory using Lorentz permittivity for the dye shell. However, in experiments, this middle peak is often not visible due to a power broadening resulting in a suppression of this middle peak [33]. Since in our case, the Mie calculations include a thick (25 nm) dye shell with high exciton number ($f_{dye} \geq 0.10$) having zero detuning with the SP mode at E_c, the observed reappearance of this middle peak is expected.

Coupling between organic molecules and SE. Now, lets assume a fully organic core-shell system having an excitonic core possessing SE mode and a generic dye shell. To study the strong light-matter coupling between organic molecules and the SE mode, we consider the TDBC J-aggregate as the core material since TDBC nanostructures are shown to support SE modes at room temperature [9, 12–17, 19]. We chose the LOM parameters for the TDBC core ($\epsilon_{core}(\omega)$) as $\epsilon_\infty = 1.45^2$, $\gamma = 0.05$ eV, $f = 0.5$, and $E_0 = 2.08$ eV to be consistent with the existing literature [19, 24], and the dye shell is modeled with the same parameters as in the case of Au core, except E_0 is tuned to 2.15 eV, as explained below. It is worth to highlight here that even though both core and shell are now made of organic materials modelled by Eq. (1), the TDBC core possesses a negative $Re\{\epsilon(\omega)\}$ regime, *i.e.*, SMR at $\sim 2.1 - 2.3$ eV as shown in Fig. 1(b), and hence, supports a SE mode along with its material absorption. However, the generic dye shell has only its material absorption and no such SE mode is supported since its $Re\{\epsilon(\omega)\}$ is always positive (*i.e.*, no SMR).

The red curve in Fig. 2(b) shows the absorption of such excitonic core having the SE mode as a strong peak at $E_c = 2.15$ eV and the material absorption of TDBC as a shoulder peak at $E_m = 2.08$ eV. To have a spectral match with the SE mode (E_c) of the TDBC core, the E_0 for the generic dye shell is set to 2.15 eV. The change in molecular concentration of the shell is modelled by varying the f in Eq. (1) for the shell (*i.e.*, f_{dye}) similar to the case of Au core. The black curve in Fig. 2(b) shows

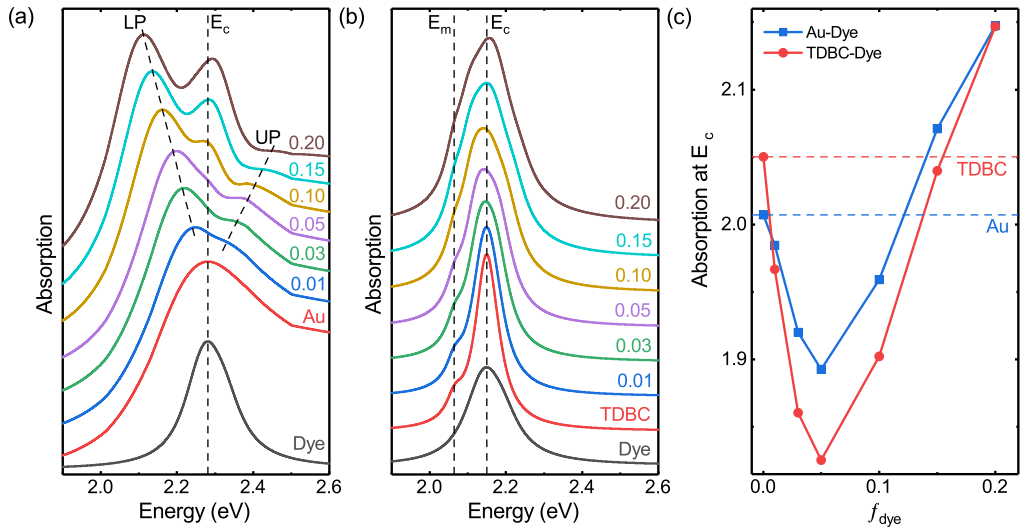

FIG. 2. (a) Absorption spectra of generic dye shell (black), Au core (red), and the core-shell coupled system for different values of f_{dye} (0.01, 0.03, 0.05, 0.10, 0.15, and 0.20) and for $\gamma = 0.1$ eV. The spectra are shifted vertically for clarity. The absorption of the dye shell is spectrally tuned to the same as the Au core absorption maximum, *i.e.*, $E_0 = E_c = 2.28$ eV (vertical dashed line). The lower (LP) and upper (UP) polariton branches are shown by the tilted black dashed lines. (b) Absorption spectra of generic dye shell (black), TDBC core (red), and the core-shell coupled system with the same γ and f_{dye} values as in (a). The spectra are shifted vertically for clarity. The SE mode of the TDBC core ($E_c = 2.15$ eV) and the material absorption of TDBC ($E_m = 2.08$ eV) are shown by the vertical dashed black lines. The absorption of the dye shell is spectrally tuned with E_c. (c) Absorption at E_c for Au-core/dye-shell ($E_c = 2.28$ eV) and TDBC-core/dye-shell ($E_c = 2.15$ eV) coupled systems as a function of f_{dye}. The blue and red horizontal dashed lines show the core absorption for Au and TDBC, respectively. The blue squares and red circles on the curves of corresponding color depict the discrete data points. In (a)-(c), absorption means absorption efficiency, *i.e.*, absorption cross-sections normalized by geometrical cross-section.

absorption of the plain shell having a spectral tuning with the SE mode of the TDBC core at $E_c = 2.15$ eV.

Considering the fact that SEs can confine and enhance light like SPs [9, 14, 15, 17, 19], one should expect strong coupling between the SE mode of the TDBC core and the generic dye shell resulting in an emergence of polariton peaks in the absorption of the coupled system. However, with an increase in f_{dye}, no such energy splitting is found for the coupled system as one can see in Fig. 2(b). The absorption around E_c is only slightly broadened as the f_{dye} increases. Apparently, such outcome hints that unlike SPs, SE mode might not be able to facilitate strong coupling.

To have a closer look, we first extract the absorption of the coupled system at E_c as a function of f_{dye} in the case of Au core (SP). As shown by the blue curve in Fig. 2(c), the absorption at E_c drops at first and then rises again. When a cavity mode and an excitonic resonance are spectrally tuned and strongly coupled to each other, new hybrid polariton states are formed on both sides, replacing the individual uncoupled states (as discussed above) and thereby, lowering the absorption, i.e., creating a transparency, at the resonance energy [22, 34, 35]. Therefore, in a strongly-coupled core-shell system, one should see creation of a transparency at the resonance energy E_c which becomes more and more prominent as the coupling becomes stronger and stronger [24]. From Fig. 2(a) it is clear that in the case of Au core (SP), a rise in f_{dye} results in an increase in strong coupling induced energy-splitting and thus, the absorption at E_c initially drops. However, for $f_{dye} \geq 0.10$, the absorption at E_c rises again due to the contribution from the non-hybridized molecular excitons as discussed before. When the absorption at E_c is calculated for the coupled system with the TDBC core (SE), we find a trend similar to the case of plasmon molecule coupling as one can see by looking at the red curve in Fig. 2(c). Furthermore, the SE mode seems to provide deeper transparency at E_c, which hints at even stronger coupling compared to the SP mode. This could be attributed to the higher quality factor [36] of the SE mode than that of the SP mode as one can see by comparing the red curves in Figs. 2(a) and 2(b). It has been shown earlier also that SE modes in excitonic nanostructures can outperform SP modes in their plasmonic analogs in terms of field-confinement (quality factor and mode volume) and coupling strength [19]. The observed transparency is also a signature of strong coupling [34, 35] and for now on we use it as the second criterion for it.

Even though the f_{dye} dependency of the core-shell absorption at E_c (Fig. 2(c)) indicates that SEs can facilitate strong coupling with deeper transparency compared to SPs, the absence of polaritons in the total absorption spectra in Fig. 2(b) is perplexing. To elucidate this, we need to remember that the polaritons are hybrid superposition states between the molecular absorption and

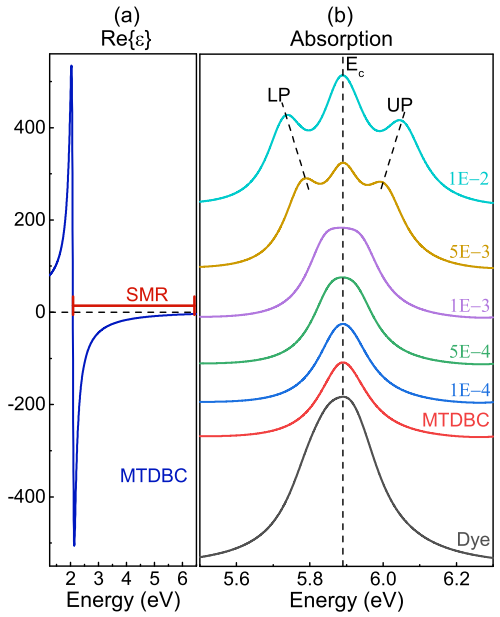

FIG. 3. (a) Real part of the dielectric function ($Re\{\epsilon(\omega)\}$) of MTDBC as a function of energy. The surface mode region (SMR), i.e., the spectral range where $Re\{\epsilon(\omega)\} < 0$ and thus the SE modes are supported, is marked in the figure. (b) Absorption spectra of generic dye shell (black), MTDBC core (red), and the core-shell coupled system for different values of f_{dye} (0.0001, 0.0005, 0.001, 0.005, and 0.01). The spectra are vertically shifted for clarity. The absorption of the dye shell is spectrally tuned to match the SE mode of the MTDBC core, *i.e.*, $E_0 = E_c = 5.9$ eV (vertical dashed line). The lower (LP) and upper (UP) polariton branches are shown by the tilted black dashed lines. In the figure, absorption means absorption efficiency, *i.e.*, absorption cross-sections normalized by geometrical cross-section.

the surface mode (SP or SE). Thus, they can exist only if the surface mode is supported, which means that they are also supported only within SMR. Let's now compare $Re\{\epsilon(\omega)\}$ profiles of Au and the TDBC core material presented in Figs. 1(a) and 1(b), respectively. For Au, the SMR of SP modes is very broad (≤ 5.96 eV) and can thus support not only the SP mode of the core, but also the polaritons around it, which appear within the spectral range of 2-2.5 eV as seen in Fig. 2(a). Therefore, the polaritons as well as the induced transparency are clearly visible in the absorption spectra. For the TDBC core, the SMR of SE modes is extremely narrow and covers only the energies $\sim 2.1 - 2.3$ eV, as one can see in Fig. 1(b). The SE mode of the excitonic core is at 2.15 eV, i.e., within SMR, and is thus supported and visible in Fig. 2(b). Similarly, the strong coupling induced transparency is well visible (Figs. 2(b) and 2(c)). Based on this, we anticipate the coupling to have similar strength (or stronger) as in the case of SP mode of the Au core and thus the polaritons to appear at about similar distances from E_c. We can now easily see that the assumed polariton energies would reside outside SMR, and most probably because of this neither supported nor visible in the absorption.

Our speculation can easily be tested by modelling a modified TDBC (MTDBC) material having negative values of $Re\{\epsilon(\omega)\}$ and thus SMR over a spectral window large enough to include the polaritons. This MTDBC is modelled by Eq. (1) with a huge oscillator strength of $f = 50$ and $\gamma = 0.1$ eV while all other LOM parameters are kept identical with the TDBC. Such a large value of f yields a very broad SMR (2.1 - 10.4 eV) for MTDBC as shown in Fig. 3(a). This is similar to the SMR of SP modes in Au. However, it is important to note here that our MTDBC material is unrealistic for J-aggregates and used here only as a proof of concept.

Now, lets consider a MTDBC core having the same geometry as Fig. 1(c). The geometry is kept the same to be able to directly compare the absorption efficiencies. However, the higher f and thus the more negative $Re\{\epsilon_{core}(\omega)\}$ pushes the energy of the SE mode to $E_c = 5.9$ eV as shown by the red curve in Fig. 3(b). The absorption of the generic dye shell is again spectrally tuned with E_c as illustrated by the black curve in Fig. 3(b) with LOM parameters: $\epsilon_\infty = 1.45^2$, $\gamma = 0.1$ eV, $E_0 = 5.9$ eV, and a varying f (f_{dye} as 0.0001, 0.0005, 0.001, 0.005, and 0.01). Note that due to increased confinement of the SE mode of the MTDBC, the system reaches the strong coupling limit already with much lower molecular absorption, *i.e.*, lower values of f_{dye}. From Fig. 3(b) it is clear that in the beginning, an increase in f_{dye} again broadens the core-shell absorption profile. For higher values of f_{dye} (0.005 and 0.01), the polariton branches emerge due to the strong coupling between organic molecules (dye shell) and the SE mode (MTDBC core). Again, the middle peak at E_c appears due to the contribution from the nonhybridized molecular excitons as discussed before. The above finding, that with a wide enough SMR of SE modes, polaritons can be sustained in a strongly coupled all-organic system, clearly validates our speculation that SE modes can facilitate strong coupling, but the polaritons might not be visible in the absorption if they reside outside the SMR of SE modes. Since such SMR is extremely narrow for majority of the excitonic materials [8, 9, 19], this draws a limitation for organic nanostructures when employed as a platform for strong coupling.

Coupling between SE and SP. To fully understand the light coupling properties of SEs, we further examine the coupling between SE and SP modes. Both modes are the so-called *resonator modes* [22] and can be used to realize strong light-matter coupling. Strong coupling between two resonator modes such as microcavity mode strongly coupled to plasmons [37] and strong coupling between two different kinds of plasmonic modes [38] have been recently realized. In this regard, strong coupling between SE and SP modes is worth exploring.

To do so, we consider again the same NP geometry as shown in Fig. 1(c) where this time, the Au core having a SP mode at $E_c = 2.28$ eV is surrounded by a

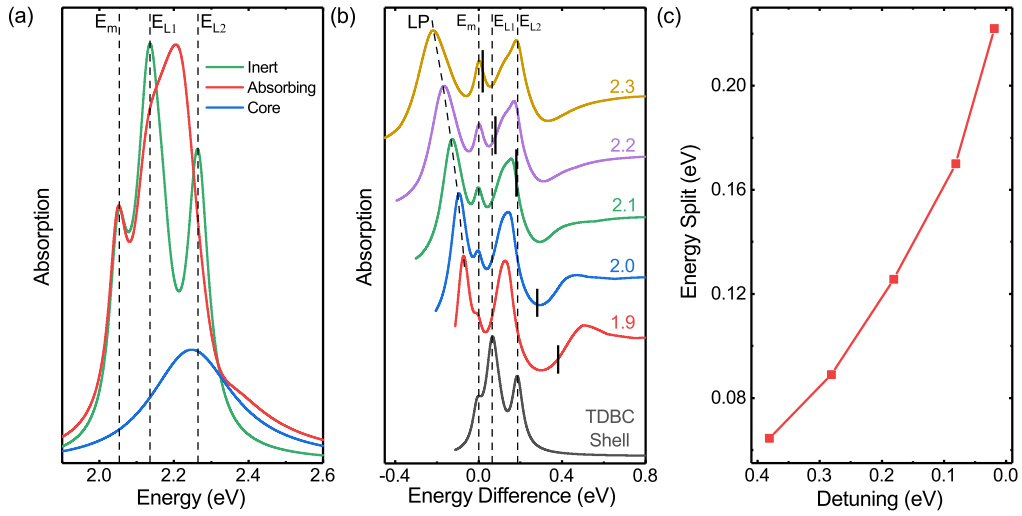

FIG. 4. (a) Absorption spectra of TDBC shell possessing two SE modes (E_{L1} and E_{L2}) along with the material absorption (E_m), when located around an inert dielectric core (green curve). An absorbing core along with the shown absorption (blue curve) yield merging of the two SE modes (red curve). (b) Absorption spectra as a function of energy difference ($E - E_m$) for the TDBC shell and the Au-core/TDBC-shell system for different values of E_m (1.9 eV, 2 eV, 2.1 eV, 2.2 eV, and 2.3 eV). On each curve (except the black one), the thick black vertical line represents the position of the SP mode of the Au core ($E_c = 2.28$ eV) on the energy difference scale. In (a)-(b), two SE modes of the TDBC shell (E_{L1} and E_{L2}) and the material absorption of TDBC (E_m) are shown by the vertical dashed black lines while in (b), the lower (LP) polariton branch is shown by the tilted black dashed line. In the figures, absorption means absorption efficiency, *i.e.*, absorption cross-sections normalized by geometrical cross-section. (c) Energy splitting ($E_m - E_{LP}$) as a function of detuning ($E_c - E_m$) where the red squares on the red curve depict the discrete data points.

TDBC shell possessing SE modes. The permittivity of the TDBC shell ($\epsilon_{shell}(\omega)$) is identical with that of the previously discussed TDBC core, while Au permittivity ($\epsilon_{core}(\omega)$) is taken from the literature [20]. A plain TDBC shell with an inert core (dielectric) yields two SE modes (E_{L1} and E_{L2}) manifested as sharp peaks along with its material absorption (E_m) in the absorption spectrum as shown by the green curve in Fig. 4(a). The origin of these two SE modes (E_{L1} and E_{L2}) comes from the interaction (Fano-type hybridization) between two individual SE modes present at the inner and outer surfaces of the TDBC shell [15]. However, if the core is absorbing (blue curve in Fig. 4(a)), like the SP mode of the Au core, these two SE modes (E_{L1} and E_{L2}) merge leading to a single broad peak as shown by the red curve in Fig. 4(a).

Since the SP mode (E_c) of the Au core cannot be changed without changing the geometry, we vary the material absorption (E_m) of the TDBC shell to study the effect of the energy difference between the SP mode and the SE modes (E_{L1} and E_{L2}). In other words, we vary the $E_m = E_0$ in Eq. (1) for TDBC shell, as 1.9 eV, 2 eV, 2.1 eV, 2.2 eV, and 2.3 eV to attain different amounts of detunings ($E_c - E_m$). In Fig. 4(b), the black curve shows the position of E_{L1}, E_{L2}, and E_m on the energy difference scale ($E - E_m$) centered at the material absorption of the TDBC shell (E_m). All other curves in the figure show the absorption of Au-core/TDBC-shell system as the function of the energy difference from the material absorption ($E - E_m$) for different values of E_m (1.9 eV, 2 eV, 2.1 eV, 2.2 eV, and 2.3 eV). On each curve in Fig. 4(b) (except the black one), the thick black vertical line represents the position of the SP mode of the Au core ($E_c = 2.28$ eV) on the energy difference scale. From the figure it is clear that for $E_m = 2.1$ eV (green curve), E_{L2} and E_c are spectrally tuned. For $E_m = 2.2$ eV (violet curve), E_{L1} and E_c are spectrally tuned, while for $E_m = 2.3$ eV (yellow curve), E_m and E_c are spectrally tuned. For E_m as 1.9 eV and 2 eV (red and blue curves), only the broad tail of the SP mode partially overlaps with E_{L1}, E_{L2}, and E_m.

From the absorption of the coupled system we can infer that in all cases (E_m as 1.9 eV, 2 eV, 2.1 eV, 2.2 eV, and 2.3 eV), E_{L1} and E_{L2} merge into a single broad peak due to the presence of an absorbing Au core like the case reported in Fig. 4(a) (red curve). In addition to the features present in TDBC shell, shown in Fig. 4(a), all the absorption curves of the coupled system (Fig. 4(b)) show a clear peak at energies lower than the material absorption (E_m). This peak moves as a function of the detuning between E_m and E_c, and its separation from E_m increases as the detuning decreases as shown in Fig. 4(c). This clearly indicates that the additional peak is the LP formed by the strong coupling between the SP mode (E_c) of the Au core and the material absorption (E_m) as in the case of Fig. 2. Like in that case, the UP is not well present here either, due to Au absorption and in particular due to interference by the SE modes. Such outcome indicates that SE modes (E_{L1} and E_{L2}) can

only weakly couple with the SP mode (E_c) while strong coupling happens only between the material absorption (E_m) and the SP mode (E_c). Considering the fact that strong coupling between different resonator modes have already been reported [37, 38], Fig. 4 clearly shows how light coupling properties of SE modes drastically differ from SP modes since strong coupling between SEs and SPs seems not possible.

To further validate our claim, we consider a scenario where, unlike in the core-shell system, SE and SP modes are not geometrically coupled. To do so, we consider a dimer system where a plasmonic Au nanobar interacts with an excitonic TDBC nanosphere. We vary the plasmon resonance of the 30 nm wide and 50 nm thick Au nanobar by changing its length from 60 to 100 nm, while keeping the 100 nm diameter TDBC nanosphere on side of the rod, 10 nm away from it. The optical response of the dimer system is computed by the finite-difference time-domain (FDTD) method [39] implemented in Lumerical [40]. For details on the dimer system and the FDTD simulations, see Supplemental Material [23].

The FDTD simulations reveal that no energy splitting is found when the SP mode is tuned with the SE mode (E_c). The energy splitting is only found when the SP mode is tuned with the material absorption (E_m) of TDBC. Such outcome is in agreement with the results reported in Fig. 4 and again confirms our claim that strong coupling happens only between the material absorption and a surface mode, SP or SE. Interestingly, we do not see any UP and only the LP branch is visible. That is most probably because the upper polaritons are spectrally overlapping with the SE mode (E_c).

It is important to highlight here that our findings on the coupling between SE and SP modes in a core-shell NP (Fig. 4) and in a dimer system (Fig. 7 in Supplemental Material [23]), interestingly, corroborate an earlier study on a similar system where strong coupling is reported only between the material absorption of a dye layer and the SP mode of a metal thin film, while the SE mode of the dye layer remains uncoupled to the SPs [11].

Conclusion. Concisely, we have studied the performance of the SE mode when employed to facilitate strong light-matter coupling. We considered a core-shell NP having a TDBC core possessing SE mode with a generic dye shell and compared it with an identical core-shell NP consisting similar dye shell with a Au core (SP mode). Our Mie calculations revealed that SE modes can facilitate strong coupling by sustaining the energy-splitting-induced transparency, which is deeper than what can be achieved using SPs. However, the polaritons are not visible in the absorption since in this case they reside outside the SMR of the SE modes. Since this SMR is extremely narrow for majority of the organic materials, our findings draw a limitation of excitonic nanostructures as a platform for strong coupling.

We further examined the coupling between SE and SP modes to explore the light coupling properties of SEs. On one hand, we considered a core-shell NP consisting a Au core having a SP mode and a TDBC shell possessing SE modes. On the other hand, we modelled a dimer system where the SP mode of a Au nanobar is interacting with the SE mode of a TDBC nanosphere. In both cases, our numerical findings showed that SE modes can only weakly couple with the SP mode, while the strong coupling happens between the excitonic material absorption and SPs. Furthermore, when the material absorption and a SP mode are strongly coupled, the SE mode can overlap with the polariton and overrun it. Our findings provide key information on the weak and strong coupling properties of SEs and hence, important in the context of developing novel excitonic devices for organic nanophotonics.

Acknowledgments. The authors are grateful to Gerrit Groenhof for helpful discussions. This work was funded by Academy of Finland (289947, 323995).

[1] D. Ballarini and S. De Liberato, Polaritonics: from microcavities to sub-wavelength confinement, Nanophotonics **8**, 641 (2019).
[2] H. Yu, Y. Peng, Y. Yang, and Z.-Y. Li, Plasmon-enhanced light–matter interactions and applications, npj Comput. Mater. **5**, 45 (2019).
[3] N. Jiang, X. Zhuo, and J. Wang, Active plasmonics: principles, structures, and applications, Chem. Rev. **118**, 3054 (2018).
[4] K. Yao and Y. Liu, Plasmonic metamaterials, Nanotechnol. Rev. **3**, 177 (2014).
[5] A. Dutta, K. Alam, T. Nuutinen, E. Hulkko, P. Karvinen, M. Kuittinen, J. J. Toppari, and E. M. Vartiainen, Influence of Fano resonance on SERS enhancement in Fano-plasmonic oligomers, Opt. Express **27**, 30031 (2019).
[6] A. Dutta and E. M. Vartiainen, Spatial localization of hotspots in Fano-resonant plasmonic oligomers for surface-enhanced coherent anti-Stokes Raman scattering, J. Eur. Opt. Soc.-Rapid Publ. **16**, 8 (2020).
[7] A. Dutta, T. Nuutinen, K. Alam, A. Matikainen, P. Li, E. Hulkko, J. J. Toppari, H. Lipsanen, and G. Kang, Fabrication-friendly polarization-sensitive plasmonic grating for optimal surface-enhanced Raman spectroscopy, J. Eur. Opt. Soc.-Rapid Publ. **16**, 22 (2020).
[8] L. Gu, J. Livenere, G. Zhu, E. E. Narimanov, and M. A. Noginov, Quest for organic plasmonics, Appl. Phys. Lett. **103**, 021104 (2013).
[9] M. J. Gentile, S. Núñez-Sánchez, and W. L. Barnes, Optical field-enhancement and subwavelength field-confinement using excitonic nanostructures, Nano Lett. **14**, 2339 (2014).
[10] A. Canales, D. G. Baranov, T. J. Antosiewicz, and T. Shegai, Abundance of cavity-free polaritonic states in resonant materials and nanostructures, J. Chem. Phys. **154**, 024701 (2021).
[11] W. J. Tan, P. A. Thomas, I. J. Luxmoore, and W. L.

Barnes, Single vs double anti-crossing in the strong coupling between surface plasmons and molecular excitons, J. Chem. Phys. **154**, 024704 (2021).
[12] K. Takatori, T. Okamoto, K. Ishibashi, and R. Micheletto, Surface exciton polaritons supported by a J-aggregate-dye/air interface at room temperature, Opt. Lett. **42**, 3876 (2017).
[13] Y. Xu, L. Wu, and L. K. Ang, Surface exciton polaritons: a promising mechanism for refractive-index sensing, Phys. Rev. Applied **12**, 024029 (2019).
[14] M. J. Gentile, S. A. R. Horsley, and W. L. Barnes, Localized exciton–polariton modes in dye-doped nanospheres: a quantum approach, J. Opt. **18**, 015001 (2016).
[15] M. J. Gentile and W. L. Barnes, Hybridised exciton–polariton resonances in core–shell nanoparticles, J. Opt. **19**, 035003 (2017).
[16] A. D. Humphrey, M. J. Gentile, and W. L. Barnes, Excitonic surface lattice resonances, J. Opt. **18**, 085004 (2016).
[17] A. Cacciola, C. Triolo, O. D. Stefano, A. Genco, M. Mazzeo, R. Saija, S. Patanè, and S. Savasta, Subdiffraction light concentration by J-aggregate nanostructures, ACS Photonics **2**, 971 (2015).
[18] S. T. Holder, C. Estévez-Varela, I. Pastoriza-Santos, M. Lopez-Garcia, R. Oulton, and S. Núñez-Sánchez, Bio-inspired building blocks for all-organic metamaterials from visible to near-infrared, Nanophotonics **12**, 307 (2023).
[19] A. Dutta and J. J. Toppari, Effect of molecular concentration on excitonic nanostructure based refractive index sensing and near-field enhanced spectroscopy, Opt. Mater. Express **13**, 2426 (2023).
[20] P. B. Johnson and R. W. Christy, Optical constants of the noble metals, Phys. Rev. B **6**, 4370 (1972).
[21] A. Dutta, V. Tiainen, H. A. Qureshi, L. Duarte, and J. J. Toppari, Modeling optical constants from the absorption of organic thin films using a modified Lorentz oscillator model, Opt. Mater. Express **12**, 2855 (2022).
[22] M. S. Rider and W. L. Barnes, Something from nothing: linking molecules with virtual light, Contemp. Phys. **62**, 217 (2021).
[23] See Supplemental Material at URL-will-be-inserted-by-publisher for details on Lorentz permittivity, Mie calculations, and FDTD simulations.
[24] G. Zengin, G. Johansson, P. Johansson, T. J. Antosiewicz, M. Käll, and T. Shegai, Approaching the strong coupling limit in single plasmonic nanorods interacting with J-aggregates, Sci. Rep. **3**, 3074 (2013).
[25] C. F. Bohren and D. R. Huffman, *Absorption and Scattering of Light by Small Particles* (Wiley-VCH, 1998).
[26] `https://www.mathworks.com/products/matlab.html`.
[27] A. Dutta, V. Tiainen, and J. J. Toppari, Numerical study on the limit of quasi-static approximation for plasmonic nanosphere, AIP Conf. Proc. **2220**, 050012 (2020).
[28] T. J. Antosiewicz, S. P. Apell, and T. Shegai, Plasmon–exciton interactions in a core–shell geometry: from enhanced absorption to strong coupling, ACS Photonics **1**, 454 (2014).
[29] F. Stete, W. Koopman, and M. Bargheer, Signatures of strong coupling on nanoparticles: revealing absorption anticrossing by tuning the dielectric environment, ACS Photonics **4**, 1669 (2017).
[30] G. Zengin, T. Gschneidtner, R. Verre, L. Shao, T. J. Antosiewicz, K. Moth-Poulsen, M. Käll, and T. Shegai, Evaluating conditions for strong coupling between nanoparticle plasmons and organic dyes using scattering and absorption spectroscopy, J. Phys. Chem. C **120**, 20588 (2016).
[31] F. Stete, P. Schoßau, M. Bargheer, and W. Koopman, Size-dependent coupling of hybrid core–shell nanorods: toward single-emitter strong-coupling, J. Phys. Chem. C **122**, 17976 (2018).
[32] W. Li, R. Liu, and X. Wang, Anomalous spectral response of plasmon-exciton strong coupling beyond J-C model, Results Phys. **31**, 105064 (2021).
[33] F. Stete, W. Koopman, C. Henkel, O. Benson, G. Kewes, and M. Bargheer, Optical spectra of plasmon-exciton core-shell nanoparticles: a heuristic quantum approach, ACS Photonics **10**, 2511 (2023).
[34] Z. Hu, X. Cui, Y. Li, X. Han, and H. Hu, Multiband tunable exciton-induced transparencies: exploiting both strong and intermediate coupling in a nanocube-hexagonal-nanoplate heterodimer J-aggregates hybrid, Opt. Express **30**, 43371 (2022).
[35] M. Mao, J. Wang, K. Mu, C. Fan, Y. Jia, R. Li, S. Chen, and E. Liang, Realizing PIT-like transparency via the coupling of plasmonic dipole and ENZ modes, Opt. Express **30**, 8474 (2022).
[36] A. Dutta, V. Tiainen, and J. J. Toppari, Optimizing geometry of low-Q all-metal Fabry-Pérot microcavity for fluorescence spectroscopy, IOPSciNotes **2**, 015205 (2021).
[37] D. G. Baranov, B. Munkhbat, E. Zhukova, A. Bisht, A. Canales, B. Rousseaux, G. Johansson, T. J. Antosiewicz, and T. Shegai, Ultrastrong coupling between nanoparticle plasmons and cavity photons at ambient conditions, Nat. Commun. **11**, 2715 (2020).
[38] B. C. Yildiz, M. Habib, A. R. Rashed, and H. Caglayan, Hybridized plasmon modes in a system of metal thin film–nanodisk array, J. Appl. Phys. **126**, 113104 (2019).
[39] S. D. Gedney, *Introduction to the Finite-Difference Time-Domain (FDTD) Method for Electromagnetics* (Morgan and Claypool, 2011).
[40] `https://www.ansys.com/products/photonics/fdtd`.

Supplemental Material for
"Weak and strong coupling properties of surface excitons"

Arpan Dutta[1,2] and J. Jussi Toppari[1]

[1]*Nanoscience Center and Department of Physics,*
University of Jyväskylä, 40014 Finland

[2]*Department of Mechanical and Materials Engineering,*
University of Turku, 20014 Finland

LORENTZ PERMITTIVITY

The complex and dispersive permittivity of the generic absorbing dye material and the excitonic material supporting the SE within a finite SMR are modelled using the Lorentz oscillator model (LOM) expressed by Eq. (1). The values of the LOM parameter used in Eq. (1) in the different cases are all listed in Tables I-IV.

TABLE I. LOM parameters for the generic dye shell surrounding the Au core used in Fig. 2(a).

parameters	dye shell for Au core
ϵ_∞	1.45^2
f	0.01, 0.03, 0.05, 0.10, 0.15, 0.20
E_0 (eV)	2.28
γ (eV)	0.10

TABLE II. LOM parameters for the excitonic TDBC core and the generic dye shell surrounding it used in Fig. 2(b).

parameters	TDBC core	dye shell for TDBC core
ϵ_∞	1.45^2	1.45^2
f	0.50	0.01, 0.03, 0.05, 0.10, 0.15, 0.20
E_0 (eV)	2.08	2.15
γ (eV)	0.05	0.10

The complex-dispersive permittivity of the excitonic TDBC shell in Fig. 4 is modelled with the same LOM parameter values reported in Table II for the excitonic TDBC core.

TABLE III. LOM parameters for the excitonic MTDBC core and the generic dye shell surrounding it used in Fig. 3.

parameters	MTDBC core	dye shell for MTDBC core
ϵ_∞	1.45^2	1.45^2
f	50	0.0001, 0.0005, 0.001, 0.005, 0.01
E_0 (eV)	2.08	5.90
γ (eV)	0.10	0.10

In Fig. 4(a), in the case of an excitonic TDBC shell with an inert core, the nondispersive dielectric constant of the core is considered as 1.45. In the case of an excitonic TDBC shell with an absorbing core, the complex and dispersive dielectric function of the core is modelled with the LOM parameter values reported in Table IV.

TABLE IV. LOM parameters for the absorbing core surrounded by the excitonic TDBC shell used in Fig. 4(a).

parameters	absorbing core
ϵ_∞	1.45^2
f	0.35
E_0 (eV)	2.20
γ (eV)	0.25

MIE CALCULATIONS

The Mie calculations are based on the Mie theory of core-shell nanosphere [25]. Lets consider the core-shell geometry shown in Fig. 5. The nanosphere has a core (radius: r_{core}) and a shell (thickness: t_{shell}). The shell outer radius is then $r_{shell} = r_{core} + t_{shell}$. The complex-dispersive refractive indices for the core and shell are $n_{core}(\lambda)$ and $n_{shell}(\lambda)$, respectively. The core-shell nanosphere is in a dielectric medium (non-dispersive refractive index n_d). For an excitation wavelength λ, the wave vector (k_d) is $k_d = 2\pi n_d/\lambda$. The Mie parameters used in the formulation are $m_1 = n_{core}/n_d$, $m_2 = n_{shell}/n_d$, $v_1 = k_d r_{core}$, $v_2 = k_d r_{shell}$, $w_1 = m_1 v_1$, $w_2 = m_2 v_1$, and $w_3 = m_2 v_2$.

The scattering (σ_{sca}), extinction (σ_{ext}), and absorption (σ_{abs}) cross-sections of the core-shell nanosphere can be derived as

$$\sigma_{sca} = \frac{2\pi}{k_d^2} \sum_{j=1}^{\infty} (2j+1)(|a_j|^2 + |b_j|^2) \tag{2}$$

$$\sigma_{ext} = \frac{2\pi}{k_d^2} \sum_{j=1}^{\infty} (2j+1) Re\{a_j + b_j\} \tag{3}$$

and

$$\sigma_{abs} = \sigma_{ext} - \sigma_{sca} \tag{4}$$

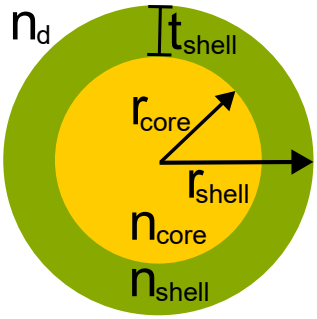

FIG. 5. Schematic of the core-shell nanosphere where core radius $r_{core} = 50$ nm, shell thickness $t_{shell} = 25$ nm, shell outer radius $r_{shell} = 75$ nm. The complex-dispersive refractive indices of core and shell are $n_{core}(\lambda)$ and $n_{shell}(\lambda)$, respectively, while $n_d = 1$ is the non-dispersive refractive index of the surrounding medium.

where a_j and b_j are the Mie coefficients. The sum over j is restricted from $j = 1$ to $j = N$ where $N = v_2 + 4v_2^{1/3} + 2$ to attain numerical convergence. The scattering (Q_{sca}), extinction (Q_{ext}), and absorption (Q_{abs}) efficiencies are then $Q_{sca} = \sigma_{sca}/c_{geo}$, $Q_{ext} = \sigma_{ext}/c_{geo}$, and $Q_{abs} = \sigma_{abs}/c_{geo}$, respectively, where c_{geo} is the geometrical cross-section of the nanosphere, i.e., πr_{shell}^2.

For a core-shell nanosphere, the Mie coefficients a_j and b_j in Eqs. (2) and (3) can be described as

$$a_j = \frac{\psi_j(v_2)[\psi_j'(w_3) - A_j\chi_j'(w_3)] - m_2\psi_j'(v_2)[\psi_j(w_3) - A_j\chi_j(w_3)]}{\xi_j(v_2)[\psi_j'(w_3) - A_j\chi_j'(w_3)] - m_2\xi_j'(v_2)[\psi_j(w_3) - A_j\chi_j(w_3)]} \tag{5}$$

$$b_j = \frac{m_2\psi_j(v_2)[\psi_j'(w_3) - B_j\chi_j'(w_3)] - \psi_j'(v_2)[\psi_j(w_3) - B_j\chi_j(w_3)]}{m_2\xi_j(v_2)[\psi_j'(w_3) - B_j\chi_j'(w_3)] - \xi_j'(v_2)[\psi_j(w_3) - B_j\chi_j(w_3)]} \tag{6}$$

with A_j and B_j as

$$A_j = \frac{m_2\psi_j(w_2)\psi_j'(w_1) - m_1\psi_j'(w_2)\psi_j(w_1)}{m_2\chi_j(w_2)\psi_j'(w_1) - m_1\chi_j'(w_2)\psi_j(w_1)} \tag{7}$$

$$B_j = \frac{m_2\psi_j(w_1)\psi_j'(w_2) - m_1\psi_j(w_2)\psi_j'(w_1)}{m_2\chi_j'(w_2)\psi_j(w_1) - m_1\psi_j'(w_1)\chi_j(w_2)} \tag{8}$$

where

$$\psi_j(x) = \sqrt{\frac{\pi x}{2}}J_{j+1/2}(x) \tag{9}$$

$$\xi_j(x) = \sqrt{\frac{\pi x}{2}}[J_{j+1/2}(x) + iY_{j+1/2}(x)] \tag{10}$$

$$\chi_j(x) = -xY_j(x) \tag{11}$$

$$\psi_j^{'}(x) = \psi_{j-1}(x) - \frac{j}{x}\psi_j(x) \tag{12}$$

$$\xi_j^{'}(x) = \xi_{j-1}(x) - \frac{j}{x}\xi_j(x) \tag{13}$$

$$\chi_j^{'}(x) = \chi_{j-1}(x) - \frac{j}{x}\chi_j(x) \tag{14}$$

and

- J_j: Bessel function of the first kind
- Y_j: Bessel function of the second kind
- ψ_j, ξ_j, and χ_j: Riccati-Bessel functions
- $\psi_j^{'}$, $\xi_j^{'}$, and $\chi_j^{'}$: first order derivatives of ψ_j, ξ_j, and χ_j

FDTD SIMULATIONS OF THE DIMER

To study the coupling between SE and SP modes in a nanostructure geometry other than the core-shell system, we consider a dimer where a plasmonic nanoantenna (Au nanobar) interacts with an excitonic nanoantenna (TDBC nanosphere) as schematically shown in Fig. 6(a). The dimensions of the Au nanobar in x, y, and z directions are L_x, L_y, and L_z, respectively. We consider $L_x = 30$ nm (width) and $L_z = 50$ nm (thickness) while L_y (length) is varied. The radius (r) of the TDBC nanosphere is taken as 50 nm and the nanosphere is kept 10 nm away from the nanobar, *i.e.*, $d = 10$ nm. The optical response of the dimer system for a plane wave excitation (normal incidence) polarized along L_y, as shown by the alignment (black arrow) of the electric-field vector ($\mathbf{E}$) in Fig. 6(a), is computed by the finite-difference time-domain (FDTD) method [39] implemented in Lumerical [40]. The complex-dispersive permittivity of the excitonic TDBC nanosphere is modelled with the same LOM parameter values reported in Table II for the excitonic TDBC core, while Au permittivity is taken from the literature [20].

In the FDTD simulation environment, at first, the dimer is designed as a geometrical object as per the schematic shown in Fig. 6(a). Then, the material properties (dielectric function) are added to the object. The substrate and superstrate are considered as air (refractive index is 1) meaning the dimer is suspended in air. Figs. 6(b) and 6(c) depict 2D and 3D views of the FDTD simulation environment in ANSYS Lumerical FDTD solver.

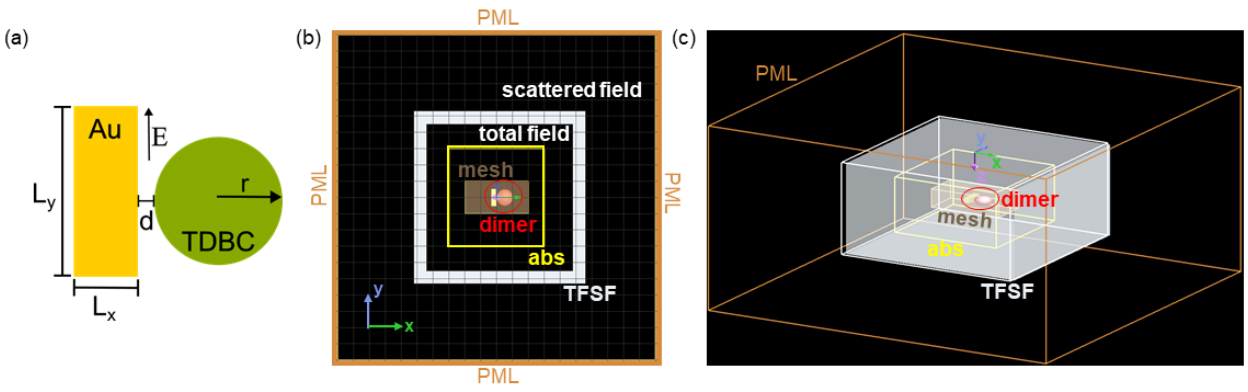

FIG. 6. (a) Schematic of the dimer where $L_x = 30$ nm, $L_z = 50$ nm, $r = 50$ nm, $d = 10$ nm, and L_y varies from 60 nm to 100 nm. The dimer is excited by normal incidence of light polarized along L_y as shown by the alignment (black arrow) of the electric-field vector (**E**). The (b) XY-view and (c) 3D-view of the FDTD simulation environment in ANSYS Lumerical FDTD solver.

As we see in the figures, the computational region is surrounded by the perfectly matched layer (PML) boundaries which absorb light without any spurious reflection. The dimer is excited by the total-field scattered-field (TFSF) source which renders plane-wave excitation of aperiodic scatterers, and separates the scattered field from the incident total field as shown in Fig. 6(b). The absorption is computed using the absorption cross-section analysis group (abs) which contains six 2D monitors forming a closed box to measure the absorbed power (net power flowing in/out of the box). The abs box monitor surrounds the dimer inside the TFSF source, i.e., inside the total field region. The simulation region is discretized non-uniformly by using a fine mesh (0.1 nm) around the dimer as shown in Figs. 6(b) and 6(c) and by coarsely discretizing elsewhere. The convergence tests are performed for non-uniform meshing to ensure numerical stability and accuracy during FDTD simulations.

The absorption spectrum of the TDBC nanosphere is presented by the black curve on the right side of Fig. 7. Like the TDBC core, reported by the red curve in Fig. 2(b), the TDBC nanosphere supports a SE mode (E_c) as a main absorption peak along with its material absorption (E_m) as a shoulder peak. The absorption spectrum of the Au nanobar for $L_y = 60$ nm is also depicted on the right side of Fig. 7 as a blue curve and it is spectrally tuned with the SE mode (E_c). We vary L_y (60 nm to 100 nm with a 5 nm increment) to shift the absorption peak of the nanobar from E_c to E_m, *i.e.*, to span through the entire absorption spectrum of the TDBC nanosphere. The dispersion of the SP mode of Au nanobar with

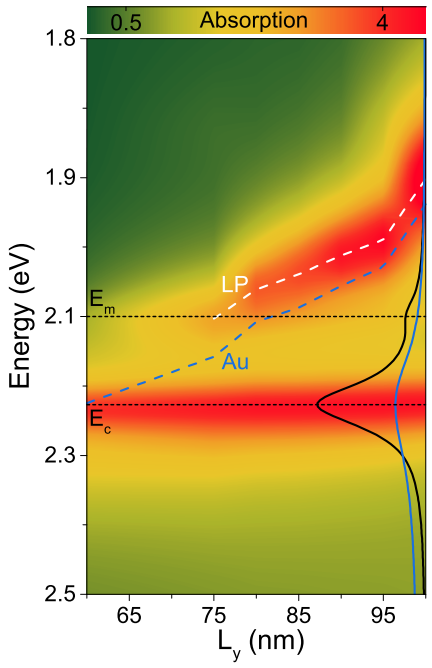

FIG. 7. Absorption of the dimer system plotted as a contour map. The black and blue curves on the right represent absorption of the TDBC nanosphere and the Au nanobar with $L_y = 60$ nm, respectively. The SE mode of the TDBC nanosphere (E_c) and the material absorption of TDBC (E_m) are shown by the horizontal dashed black lines. The blue and white dashed lines depict the dispersion of the SP mode in Au nanobar and the lower polariton (LP) branch originated due to strong coupling of E_m with the SP mode, respectively. In the figure, absorption means absorption efficiency, *i.e.*, absorption cross-sections normalized by geometrical cross-section.

respect to L_y is shown by the blue dashed line in Fig. 7.

The absorption of the coupled (dimer) system plotted as a contour map in Fig. 7 reveals that no energy splitting is found when the SP mode is tuned with the SE mode (E_c). The energy splitting is only found when the SP mode is tuned with the material absorption (E_m) of TDBC and as a consequence, a polariton branch (LP) emerges as shown by the white dashed line in Fig. 7. Such outcome is in agreement with the results reported in Fig. 4 and again confirms our claim that the strong coupling happens only between the material absorption and SPs. Interestingly, in Fig. 7, we do not see any upper polariton branch and only the LP branch (white dashed line) is visible. That is most probably because the upper polaritons are spectrally overlapping with the SE mode (E_c).